Insights into Enzyme Function from Studies on Mutants of Dihydrofolate Reductase

S. J. BENKOVIC, C. A. FIERKE, A. M. NAYLOR

Kinetic analysis and protein mutagenesis allow the importance of individual amino acids in ligand binding and catalysis to be assessed. A kinetic analysis has shown that the reaction catalyzed by dihydrofolate reductase is optimized with respect to product flux, which in turn is predetermined by the active-site hydrophobic surface. Protein mutagenesis has revealed that specific hydrophobic residues contribute 2 to 5 kilocalories per mole to ligand binding and catalysis. The extent to which perturbations within this active-site ensemble may affect catalysis is discussed in terms of the constraints imposed by the energy surface for the reaction.

DIHYDROFOLATE REDUCTASE (5,6,7,8-TETRAHYDROFOLATE: NADP oxidoreductase, E.C. 1.5.1.3) catalyzes the NADPH-dependent reduction of 7,8-dihydrofolate (H_2F) to 5,6,7,8-tetrahydrofolate (H_4F). The enzyme is necessary for maintaining intracellular pools of H_4F and its derivatives, which are essential cofactors in the biosynthesis of purines, thymidylate, and several amino acids. It is the target enzyme of a group of antifolate drugs, methotrexate (MTX), trimethoprim, and pyrimethamine, that are widely used as antitumor and antimicrobial agents (*1*).

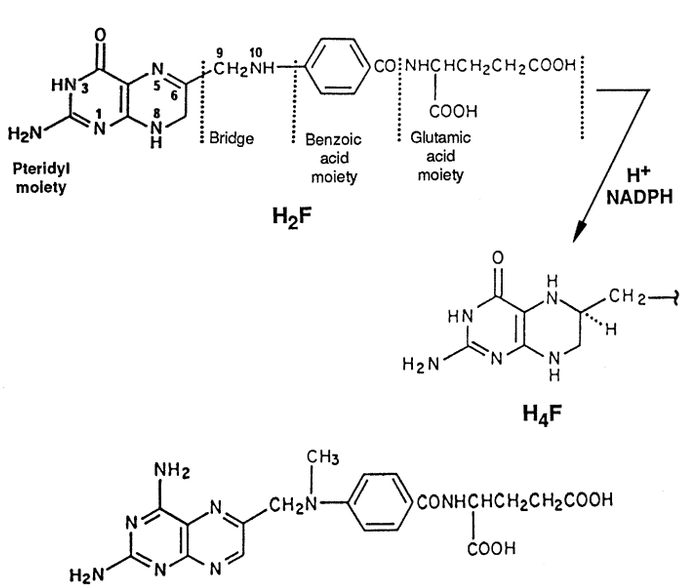

The identities of the amino acids at the active site of dihydrofolate reductase (DHFR) are now known, but the function and relative importance of the amino acid residues in binding and catalysis have not been clarified. We have used site-directed mutagenesis to establish structure-function relations for the *Escherichia coli* DHFR and in particular to evaluate the importance of hydrophobic amino acids on the function of this enzyme and on the binding of inhibitors.

The nature of the question posed presupposes two important sets of data (*2*): (i) an accurate structure that closely approximates the enzyme·H_2F·NADPH reactive ternary complex so that the key amino acid contacts are revealed and (ii) the elucidation of a complete kinetic pathway that can explain the steady-state behavior of DHFR in terms of the rate-limiting steps in turnover under a variety of conditions and that allows for direct measurement of the catalytic step at the enzyme-active site.

Structure

Visualization of the active-site amino acids was provided by the x-ray diffraction studies of Matthews *et al.* (*3*) on crystals of the *E. coli* DHFR·MTX complex and of the *Lactobacillus casei* DHFR·MTX·NADPH ternary complex (*4, 5*) refined to 1.7 Å (*6, 7*). The two backbone structures are similar, despite less than 30% homology for the two sequences; when the coordinates of 142 of the α-carbon atoms (out of 159) of the *E. coli* DHFR are matched to the structurally equivalent carbons of the *L. casei* DHFR, the root-mean-square deviation is only 1.07 Å (*6*). The active site of both proteins is a cavity ~15 Å deep that is lined by hydrophobic side chains; the only polar side chain is the carboxyl group of Asp^{27} (*E. coli*) (Fig. 1). NADPH binds in an extended conformation with the nicotinamide moiety inserted through the entrance of the cavity where it makes hydrophobic and hydrogen-bonding interactions with residues on the bottom and sides of the site. Methotrexate binds in an open conformation with the pteridine ring nearly perpendicular to the benzoyl ring. The pyrimidine edge of the pteridine ring is deeply buried in the active site, whereas the glutamate side chain extends out of the cavity to the surface. Selected key hydrophobic contacts are also illustrated in Fig. 1. The same interactions have been built into the proposed enzyme·NADPH·H_2F complex (*6*) but with the pteridine ring turned over with respect to the side chain by a 180° rotation about the C6–C9 bond, as demanded by the stereochemical course of the reduction (*8*). However, Naylor and Goddard (*9*) have suggested, with the use of molecular mechanics calculations, that the energetics of these alternate forms are nearly equal (within a few kilocalories) for both H_2F and MTX bound to DHFR. The two complexes serve as the basis for our selection of residues for mutation.

S. J. Benkovic is in the Department of Chemistry, Pennsylvania State University, University Park, PA 16802. C. A. Fierke is in the Department of Biochemistry, Duke University Medical Center, Durham, NC 27710. A. M. Naylor is in the Department of Chemistry, California Institute of Technology, Pasadena, CA 91125.

Fig. 1. Carbon backbone structure of *E. coli* DHFR including bound ligands (MTX and NADPH) and the side chains for key amino acids [depicted with BIOGRAF (*25*)].

Kinetics

The kinetic sequence for *E. coli* DHFR that predicts steady-state kinetic parameters and full-time course kinetics under a variety of substrate concentrations and *p*Hs was established by measuring the various ligand association and dissociation rate constants and pre-steady-state reaction transients with the use of stopped-flow fluorescence and absorbance spectroscopy (*10*). The scheme at 25°C is shown in Fig. 2, where NH = NADPH and N = NADP. Several key features relevant is our discussion are: (i) steady-state turnover is limited at *p*H 6 to 7 by H_4F release; (ii) dissociation of H_4F is fastest from the mixed ternary E·NH·H_4F complex; consequently the kinetic pathway for steady-state turnover at saturating substrate concentrations follows a specific, preferred pathway, in which H_4F dissociation from DHFR occurs after NADPH replaces NADP so that the catalytic cycles are interlocked (heavy arrows); and (iii) the reaction strongly favors H_4F formation (overall equilibrium constant $K_{ov} \approx 10^4$, *p*H 7) that is partially reflected in the internal equilibrium E·NH·$H_2F \rightleftharpoons$ E·N·H_4F (internal equilibrium constant $K_{int} \approx 10^3$, *p*H 7) for the reactive ternary complexes.

Examination of the *p*H dependence of these reactions established an active-site group with an intrinsic pK_a of 6.5 for the E·NH·H_2F ternary complex—a value that is the same for all forms of the enzyme: free, binary, and ternary complexes (*11–13*). Protonation of this group is required for the chemical step that involves hydride transfer from NH to H_2F. This active-site group is most likely Asp^{27}. Replacement of the Asp^{27} by Asn or Ser generates new enzyme forms that do not have an acidic proton at their catalytic site and that require preprotonated H_2F for activity (*14*). However, because of the location of the carboxyl of Asp^{27}, its proton cannot directly transfer to N5 of H_2F and requires a pathway through intervening water molecules or possibly O4 of H_2F (*15*). Although the proton transfer component of the reduction step is thermodynamically unfavorable [pK_a (Asp^{27}) = 6.5; pK_a (N5 of H_2F) = 3.8 (*16*)], the calculated proton transfer rate, 2×10^7 sec^{-1}, provides a sufficient concentration of protonated H_2F so that the observed rate for reduction (950 sec^{-1}) is not rate-limiting.

Free Energy Profiles

The detailed descriptions of reactions in terms of free energy profiles have provided impressive insights into the coupling between the overall thermodynamic free energy change for the given reaction and specific steps in the kinetic sequence for enzyme turnover (*17, 18*). The free energy profiles provide a quantitative comparison between the ground and transition state levels for enzyme-ligand complexes (*19–21*).

Before we consider the effect of site-specific mutations on the characteristics of DHFR, we evaluate the efficiency of this enzymic process. Given the definition of the kinetic sequence under physiological conditions (we introduce concentrations for NH, N, H_4F, and H_2F that approximate those of the *E. coli* cell), we can calculate the steady-state turnover under these conditions. A hypothetical maximum turnover is set by having as the rate-limiting step the diffusional binding of H_2F to E·NH (*22*), because the higher concentration of NH would maintain the reductase in the E·NH form. Under these conditions the enzyme is operating at 15% of its hypothetical maximum turnover, slightly limited by the dissociation of H_4F from E·NH·H_4F. [This efficiency could be less if, under cellular conditions, channeling of H_2F to the enzyme occurred (*23*).] Consequently, the division of the free energy change for the DHFR-catalyzed reaction into the steps in Fig. 3 is a satisfactory solution to the problem of catalyzing this process intracellularly.

There are a number of pathways that efficiently solve the energetics of the reduction within the thermodynamic constraints imposed by the overall reaction equilibrium and the diffusional barrier of substrate-enzyme combination. All of these solutions have two features in common: (i) the energy levels of the reaction intermediates are above that of the product ground state and (ii) the intermediate transition state energy levels are below those for forming the E·NH·H_2F complex.

One solution is equivalent to stabilizing equally all of the intermediate ground and transition states relative to a primitive reaction pathway, a process designated as uniform binding (*17*). The DHFR kinetic scheme conforms to within 1.6 kcal mol^{-1} to the predictions of the uniform binding constraint. Moreover, the internal states, E·NH·H_2F and E·N·H_4F, need not be at the same energy level for high catalytic efficiency (*21, 24*) because of the apparent irreversibility of the overall conversion. Simulations predict that this internal equilibrium constant can vary by 10^3 with less than a twofold change in turnover efficiency when the uniform binding constraint is maintained (*20*). An important consequence of the high efficiency of the wild-type enzyme is that mutations generally will decrease the flux of the reductase reaction under physiological conditions.

Comparison of *E. coli* and *L. casei* DHFRs

We have studied two kinds of mutants, those that occur naturally as in the comparison of the *E. coli* and *L. casei* enzymes and those generated through site-specific mutagenesis at the active site of the *E. coli* enzyme.

The active-site amino acids of the two bacterial DHFRs were overlaid with MTX as a center for alignment; their solvent-accessible surfaces were displayed with BIOGRAF (Fig. 4) (*25*). All of the residues that contained any atom within 5 Å of MTX were included. The active-site amino acid homology was computed to be 55% from a base ensemble of 40 amino acids; those that were either identical or have only backbone interactions were deemed homologous. As a calibration point, the solvent-accessible surface of MTX in the binary *E. coli* and ternary *L. casei* complexes is identical (±2%).

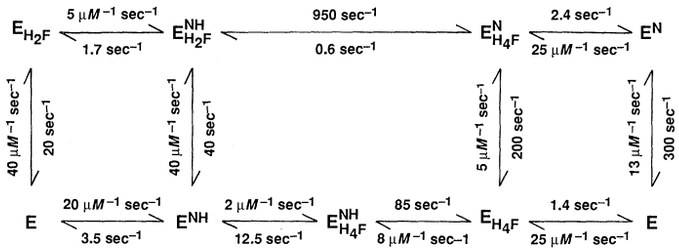

Fig. 2. Kinetic scheme for dihydrofolate reductase at 25°C, MTEN buffer; N, NADP; NH, NADPH; H_2F, dihydrofolate; H_4F, tetrahydrofolate.

Comparison of the total area of the solvent-accessible surfaces of the two proteins within 5 Å of the MTX revealed that the *E. coli* area is 93% that of *L. casei* (after deletion of the residues 15 to 20 in *L. casei* that are positioned by NADP). The congruence in the protein surface in the region of MTX is remarkably similar; discernible differences occur, however, near the glutamate and benzoyl residues (Fig. 4).

Consistent with the apparent similarities in protein-substrate interactions are the kinetic schemes of the two enzymes, which are nearly identical and feature rapid, essentially irreversible hydride transfer followed by rate-limiting H_4F dissociation from E·NH·H_4F, as described previously for the *E. coli* enzyme. A comparison of the reaction coordinate diagrams for the two enzymes under physiological conditions is shown in Fig. 3 (*26*). The major difference observed is that the free energy for binding NADPH to the *L. casei* enzyme is 2 kcal mol^{-1} more favorable than the *E. coli* enzyme, whereas the remainder of the free energy differences are less than 1 kcal mol^{-1}. We presume that NADPH is positioned identically on both enzymes.

We conclude that the energy levels of ground and transition state species are predetermined by interactions between the substrate and the active-site surface, which can be constructed by a variable combination of amino acids. This analysis does not preclude specific transition state stabilization (*27, 28*) that arises from changes on the protein surface as the reaction proceeds; obviously both the DHFR from *E. coli* and *L. casei* can respond similarly. The design of species-specific inhibitors should exploit specific regions where obvious differences are manifest, that is Ile^{50} (*E. coli*) versus Phe^{49} (*L. casei*).

Site-Specific Mutants

In the study of designed mutant proteins, an important initial question to address is their structural integrity. Recent crystallographic studies indicate that point mutations are in general accommodated by very minor readjustments of the tertiary protein structure with water molecules occupying the space created by a smaller amino acid α side chain (*14, 29, 30*). In the case of the *E. coli* DHFR, x-ray crystallographic studies of the Asn^{27} and Ser^{27} mutants showed that neither the MTX binding geometry nor the detailed three-dimensional topography of the enzyme was altered by the mutation (*14*). A kinetic analysis of the conformational states of various reductase mutants generated at the sites depicted in Fig. 1 established that the distribution and rate of interconversion of the two conformational states of the free and mutant enzymes were generally unchanged (*31–33*). We conclude that our mutants have the same basic conformation as the wild type and that changes in their binding and catalytic properties can be attributed primarily to the altered amino acid, but we note that substitution leads to localized conformational changes as the protein structure readjusts (*34*) and thus requires a cautious interpretation of any data (vide infra).

We consider mutations at three strictly conserved amino acids (Phe^{31}, Leu^{54}, and Thr^{113}). Phe^{31} resides in a hydrophobic pocket and interacts with the pteroyl moiety of H_2F through van der Waals contacts such that the edge of the phenyl ring is oriented toward faces of both the pteridine ring and *p*-aminobenzoyl group (*7*) in an edge-to-face aromatic-aromatic interaction (*35*). The isobutyl side chain of Leu^{54} is part of a hydrophobic region around the benzoyl glutamate portion of the H_2F but is more than 10 Å distant from the site of hydride transfer. The hydroxyl of Thr^{113} forms a hydrogen bond to the carboxylate oxygen of Asp^{27} and interacts with the 2-amino group of the pteridine moiety through a hydrogen-bonded water, 201. The effects of these mutations on key rate steps in dihydrofolate reductase turnover are exhibited in Table 1. There are a number of salient changes: (i) the dissociation constants for H_2F and H_4F increase with a diminution in the bulk of the α substituent at Phe^{31} and Leu^{54} as well as the loss of the hydrogen-bonding interaction at Thr^{113}; (ii) the maximum velocity V_M increases by a factor of 2 to 3 as a consequence of increasing k_{off} (the dissociation rate constant of H_4F from E·NH·H_4F); (iii) the rate constant for the hydride transfer step (k_H) decreases with the Gly^{54} and the [Gly^{54}, Val^{31}] mutants so that it is rate-limiting for turnover; and (iv) increases in the dissociation constants for MTX qualitatively parallel those for H_2F and H_4F. Although these mutant enzymes have larger V_M values, the smaller binding constants for H_2F ($1/K_{H_2F}$) lower their turnover in a cellular milieu where the concentration of H_2F is estimated to be 0.3 μ*M*.

From a comparison of various mutants to the wild-type protein one may estimate the contribution of a side chain group from the free energy of substrate or inhibitor binding (*36*). For example, the replacement of Leu^{54} with Gly^{54}, which is the closest approach to the complete deletion of the isobutyl side chain, may provide an estimate of the hydrophobic binding energy of this side chain. A set of these free energy changes is shown in Table 2. A difficulty with this approach is that the deletion will most certainly alter the architecture within the active site. For example, the effect of a glycine substitution is to increase the degrees of freedom of neighboring residues, and in addition, water molecules may now begin to occupy the cavity. More rigorously, let G^N_E and G^N_C be the free energy of the enzyme and the enzyme-substrate complex, respectively, for the equilibrium binding of A to wild-type (N = Y) and mutant (N = H) DHFRs so that:

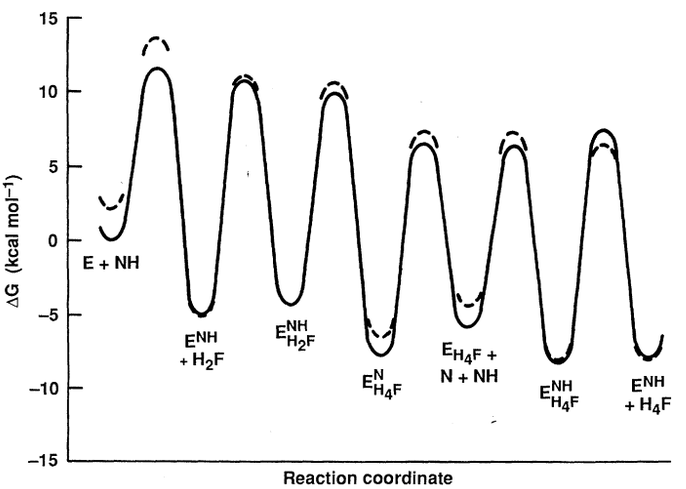

Fig. 3. Gibbs free energy coordinate diagrams for *E. coli* (———) and *L. casei* (– – –) dihydrofolate reductase aligned at the substrate ternary complex, E·NH·H_4F, calculated for conditions approximating a bacterial cell: 1.0 m*M* NADPH, 1.5 m*M* NADP, 0.3 μ*M* H_2F, 13 μ*M* H_4F, and 0.1*M* NaCl, *p*H 7.0, 25°C.

$$E^Y + A \rightleftharpoons E^Y \cdot A \qquad \Delta G_1 = G_C^Y - G_E^Y - G_A \qquad (1)$$

$$E^H + A \rightleftharpoons E^H \cdot A \qquad \Delta G_2 = G_C^H - G_E^H - G_A \qquad (2)$$

$$\text{Then: } \Delta(\Delta G)_{obs} = G_C^Y - G_C^H - G_E^Y + G_E^H = \Delta G_C^{Y,H} - \Delta G_E^{Y,H} \qquad (3)$$

The ground-state free energies of the enzymes may or may not be identical ($\Delta G_E^{Y,H} \neq 0$), nor is it obvious when this term can be safely neglected; thus $\Delta\Delta G_{obs}$ may not equal the intrinsic binding energy $\Delta G_C^{Y,H}$ contributed by group Y. A similar situation prevails for the measurement of hydrogen bond strength, where one must distinguish between apparent and intrinsic binding energies (*37*).

In terms of apparent binding energies, Leu^{54} contributes 3.9 and 5.0 kcal mol^{-1} to the respective binding of H_2F and MTX to the *E. coli* DHFR, emphasizing the greater importance of hydrophobic interactions in general (Table 2) (*38*) relative to salt bridge formation between the 2-amino group of MTX and Asp^{27}, which has been estimated to be ~1.8 kcal mol^{-1} (*14*). The same ordering, that is, hydrophobic forces are greater than electrostatic forces, for MTX binding emerges from free energy perturbation calculations (*39*). The free energy changes for the Phe^{31} and Val^{31} mutant additionally include loss of the edge-to-face weakly polar interaction between the aromatic side chain and the ligand, and in fact may be the major factor contributing to this $\Delta\Delta G$ of 2 to 3 kcal mol^{-1}. In the case of Tyr^{31}, the loss of binding affinity may reflect difficulties in solvating as well as accommodating the hydroxyl in the binary complex. The fact that $\Delta\Delta G$ for the double mutant is less than the sum of $\Delta\Delta G$ for the two single mutants indicates the absence of large structural unfolding (*40*).

Free Energy Relations

Although these changes are made at three spatially separate loci on the surface of the active site, they can be related by means of a linear free energy structure-function correlation of the type $k = CK^{\beta}$ that links thermodynamic with kinetic changes. In particular Fersht and his co-workers have applied these relations to mutants of tyrosyl–transfer RNA (tRNA) synthetase (*41*). In principle the free energy change between the reactant ground state and transition state ($\Delta\Delta G\dagger$) is correlated to the corresponding free energy change for the reactant-product equilibrium ($\Delta\Delta G$), relative to a standard reactant. Generally such plots are linear with slopes between zero and one. In the present case, however, the slope of a plot of log k_H (the rate of hydride transfer) versus log k_H/k_{-H} (the internal equilibrium) for a series of DHFR mutants is nearly vertical (>>1), suggesting that the transition state stability is sensitive to the mutation (the values of k_H decreased) but that the equilibrium involving the ground states is not. This implies that the reactant and product ground state are perturbed to the same extent—a manifestation of the uniform binding noted earlier. An alternate explanation that the perturbation is confined entirely to a particular transition state stabilization is ruled out by the effects of these mutations on the dissociation of H_2F and H_4F.

A variant on the classical free energy correlation relates changes in rate constants to changes in a second property of a common reactant. In the present case, plots of log k_H versus log K_{H_2F} (Fig. 5) are linear with slopes of unity and suggest that the perturbation caused by these mutations is twice as important in altering the free energy of the transition state for hydride transfer as compared with the ground state of the $E \cdot H_2F$ complex. The important point here is that the rate of hydride transfer increases in direct proportion to an increase in the affinity of the reductase for H_2F, with the wild-type enzyme affinity being maximal.

An interpretation of the collective data is that the active site is a reactive surface whose major function is to constrain the NADPH and the H_2F into an optimal reaction space and orientation. This is not a new concept; certainly the effect of extensive mutations on tyrosyl-tRNA synthetase (*42*), subtilisin (*43*), as well as alterations in substrate structure (*44*), show that all active-site groups contribute to varying extents to selective binding of substrates and to catalysis. These groups, that is, Leu^{54}, can be some distance from the reaction site and still have a pronounced influence. Moreover, the effects of the mutation should be more pronounced on the kinetic rather than the thermodynamic parameters since the former requires precise alignment of the NADPH and H_2F, whereas the latter do not. Eventually a situation can be reached when further increases in the binding affinity for H_2F do not translate into an increased rate (k_H), hence the negative deviation for the wild-type DHFR from the correlation in Fig. 5.

A key question, therefore, is the relation between the energetics of the reaction path, in this case the transfer of a hydride ion between C4 of the dihydropyridine and C6 of H_2F, as a function of the distances and angles of the three participating atoms (–C · · · H · · · C=). The construction of a molecular potential hypersurface defining the minimal energy path between the stable ground-state species either from experimental data or from theoretical calculations remains a formidable task. Chemical reaction dynamic information has been extracted from crystallographic data; two notable examples are the hydrolysis of alkylaryl acetals and the addition of nitrogen nucleophiles to carbonyls. An increase of only 0.01 Å in the ground-state length of the acetal bond to be cleaved is equivalent to a decrease of ~3 kcal mol^{-1} in the activation energy (*45*). For nucleophiles the angle of approach to the carbonyl clusters is near 105° (*46*). Houk and co-workers have located the transition states for hydride transfer from either methylamine or 1,4-dihydro-

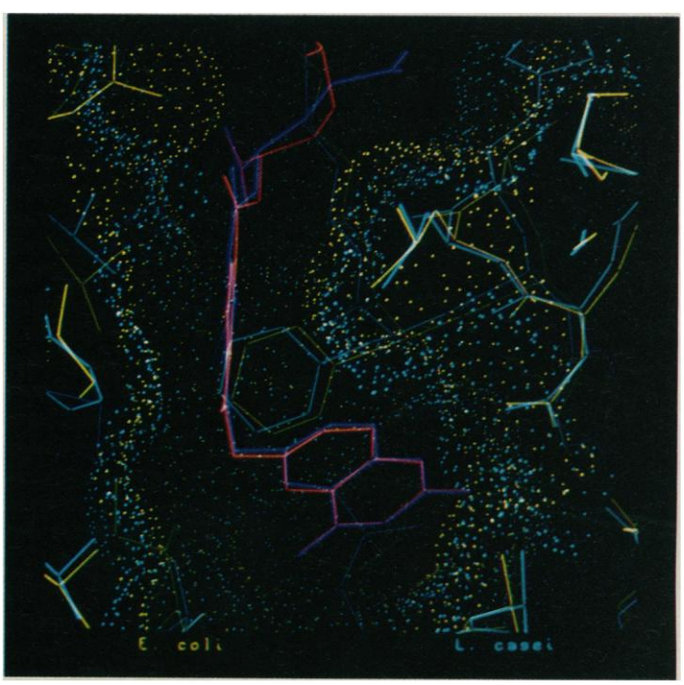

Fig. 4. Superpositioning of the active sites of the *E. coli* (gold) and *L. casei* (blue) DHFRs with MTX as a center for alignment. All residues within 5 Å of the MTX were included. Key residues that are visible in the figure (*E. coli: L. casei*) include Leu^{28}:Leu^{27} (upper right); Asp^{27}:Asp^{26} (middle right); Ala^{7}: Ala^{6} (lower right); Thr^{46}:Thr^{45} (lower left); Ile^{50}:Phe^{49} (middle left); and Arg^{52}:Leu^{51} (upper left). Phe^{31} can be seen in the center of the view [depicted with BIOGRAF (*25*)].

Fig. 5. Free energy correlation diagram relating the rate constant for hydride transfer to the K_D for dissociation of H_2F from a series of mutants in the folate binding site of DHFR.

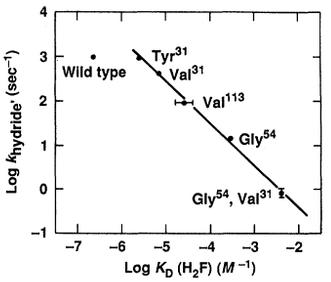

Table 1. Effects of mutations on kinetic and thermodynamic parameters characteristic of *E. coli* DHFR (*10, 12, 32, 48*).

E. coli DHFR	k_H* (sec^{-1})	k_{off}* (H_4F) (sec^{-1})	V_M* (sec^{-1})	K_D (H_4F) (μM)	K_D (H_2F) (μM)	K_D (MTX) (nM)
Wild type	950	12	12	0.06	0.21	0.02
Val^{31}	400	> 20	26	0.3	6.6	3.2
Gly^{54}	14	>300	14	>15	140	100
Gly^{54}, Val^{31}	0.9	>300	0.9		2000	900
Val^{113}	120	60	32	4.0	30	0.5

*pH-independent values in MTEN buffer, 25°C.

Table 2. Free energy changes associated with ligand binding to *E. coli* DHFR. The error for these values (SEM) is ±0.5 kcal mol^{-1}.

Mutation	Change	K_D (H_2F) $\Delta\Delta G$ (kcal mol^{-1})	K_D (MTX) $\Delta\Delta G$ (kcal mol^{-1})
Phe^{31} to Tyr	Hydrophobic	1.5	2.7
Phe^{31} to Val	Hydrophobic	2.0	3.0
Leu^{54} to Gly	Hydrophobic	3.9	5.0
Phe^{31} to Val, Leu^{54} to Gly	Hydrophobic	5.4	6.3
Thr^{113} to Val	Hydrogen bond (*2*)	2.9	1.9

pyridine to the methyliminium cation. In either case a syn transition state is favored with a bent –C···H···C= bond angle (150° to 160°) (*47*).

These conclusions may be transposed to the DHFR reaction subject to the restrictions imposed by stereochemical considerations, so that a model emerges as a possibility for the chemical reduction step.

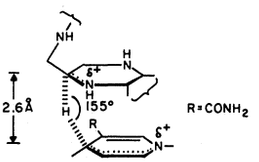

From their theoretical calculations, the optimal carbon-carbon bond distance in this transition state is 2.6 Å; extending this distance by 0.1 or 0.3 Å causes increases in the energy of activation of 0.7 and 5.0 kcal mol^{-1}, respectively (*48*). These energy differences translate into a reduction in the rate of the hydride transfer step by factors of 3 to 5000. Thus the information gleaned from either experiment or theory argues for the importance of small molecular changes on the order of <1 Å that can account for the observed changes caused by specific mutations. On the other hand, we cannot eliminate at present the possibility that the mutated enzymes have allowed the formation of nonproductive ground-state complexes, such as bound H_2F adopting the MTX conformation (*9, 49*).

Conclusions

Insights into the importance of active-site residues in the binding of ligands and in catalysis have been obtained through the powerful combination of site-specific mutagenesis and complete kinetic analysis of the enzyme-catalyzed transformation. Hydrophobic interactions appear to dominant the binding of substrates or inhibitors as well as catalysis. The disparate mutations studied to date fit structure-reactivity correlations that linearly relate the rate of hydride transfer to the binding of H_2F, which is consistent with the hypothesis that the active-site residues act as an ensemble to create a particular surface for binding and catalyzing the reaction. The same surface can be constructed by differing combinations of amino acids, as illustrated by the *E. coli* and *L. casei* comparison, and can be unfavorably perturbed by single changes at key residues. Consequently there must be compensating changes. Information obtained from both theory and experiment document that small changes in distance may be translated into energy changes sufficient to account for our observations. These changes, on the order of <1 Å, most likely will not be detected by the present methods (x-ray and nuclear magnetic resonance) used to establish structure and these methods may only detect changes in mutated enzymes largely devoid of activity. Furthermore, one can anticipate that linearity in the structure-reactivity correlations will decay, since the correlation between the free energy of activation and reactant bond angle and distances must ultimately be nonlinear, and because the requirements for ligand binding are not as restrictive as those for catalysis.

REFERENCES AND NOTES

1. R. L. Blakley, in *Folates and Pterins* R. L. Blakely and S. J. Benkovic, Eds. (Wiley, New York, 1985), vol. 2, p. 191.
2. J. R. Knowles, *Science* **236**, 1252 (1987).
3. D. A. Matthews *et al.*, *ibid.* **197**, 452 (1977).
4. D. A. Matthews *et al.*, *J. Biol. Chem.* **253**, 6946 (1978).
5. D. A. Matthews, R. A. Alden, S. T. Freer, N. Xuong, J. Kraut, *ibid.* **254**, 4144 (1979).
6. J. T. Bolin, D. J. Filman, D. A. Matthews, R. C. Hamlin, J. Kraut, *ibid.* **257**, 13650 (1982).
7. D. J. Filman, J. T. Bolin, D. A. Matthews, J. Kraut, *ibid.*, p. 13663.
8. P. A. Charlton, D. W. Young, B. Birdsall, J. Feeney, G. C. K. Roberts, *Chem. Commun.* **1979**, 922 (1979).
9. A. M. Naylor and W. A. Goddard III, unpublished results.
10. C. A. Fierke, K. A. Johnson, S. J. Benkovic, *Biochemistry* **26**, 4085 (1987).
11. S. R. Stone and J. F. Morrison, *Biochim. Biophys. Acta* **745**, 247 (1983).
12. J.-T. Chen, K. Taira, C. D. Tu, S. J. Benkovic, *Biochemistry* **26**, 4093 (1987).
13. K. Taira, J.-T. Chen, C. A. Fierke, S. J. Benkovic, *Bull. Chem. Soc. Jpn.* **60**, 3025 (1987).
14. E. E. Howell, J. E. Villafranca, M. S. Warren, S. J. Oatley, J. Kraut, *Science* **231**, 1123 (1986).
15. J. E. Gready, *Biochemistry* **24**, 4761 (1985).
16. M. Poe, *J. Biol. Chem.* **252**, 3724 (1977).
17. W. J. Albery and J. R. Knowles, *Biochemistry* **15**, 5631 (1976).
18. W. P. Jencks, *Adv. Enzymol.* **43**, 219 (1975).
19. J. Stackhouse, K. P. Nambiar, J. J. Burbaum, D. M. Stauffer, S. A. Benner, *J. Am. Chem. Soc.* **107**, 2757 (1985).
20. C. A. Fierke, R. D. Kuchta, K. A. Johnson, S. J. Benkovic, *Cold Spring Harbor Symp. Quant. Biol.*, in press.
21. J. Chin, *J. Am. Chem. Soc.* **105**, 6502 (1983).
22. M. H. Penner and C. Frieden, *J. Biol. Chem.* **262**, 15908 (1987).
23. M. Young, G. Wasserman, P. Benkovic, S. Benkovic, in *Proceedings of the Second Workshop on Folyl and Antifolyl Polyglutamates*, I. Goldman, Ed. (Praeger, New York, 1985), p. 76.
24. A. D. Ellington and S. A. Benner, *J. Theor. Biol.*, in press.
25. BIOGRAF is an interactive molecular stimulation three-dimensional graphics program from BIODESIGN, Inc., Pasadena, CA.
26. J. Andrews and C. A. Fierke, unpublished results.
27. L. Pauling, *Chem. Eng. News* **24**, 1375 (1946).
28. D. E. Koshland and K. E. Neet, *Annu. Rev. Biochem.* **37**, 359 (1967).
29. S. Sprang *et al.*, *Science* **237**, 905 (1987).
30. C. Chothia, *J. Mol. Biol.* **105**, 1 (1976).
31. P. J. Cayley, S. M. J. Dunn, R. W. King, *Biochemistry* **20**, 874 (1981).
32. R. J. Mayer, J.-T. Chen, K. Taira, C. A. Fierke, S. J. Benkovic, *Proc. Natl. Acad. Sci. U.S.A.* **83**, 7718 (1986).
33. J.-T. Chen, R. J. Mayer, C. A. Fierke, S. J. Benkovic, *J. Cell. Biochem.* **29**, 73 (1985).
34. J. A. Gerlt, D. W. Hibler, J. A. Wilde, P. H. Bolton, *Protein Engr.* **1**, 233 (1987).
35. S. K. Burley and G. A. Petsko, *Science* **229**, 23 (1985).

36. A. R. Fersht, in *Enzyme Structure and Mechanism* (Freeman, New York, ed. 2, 1985), p. 311.
37. ———, *Trends Biochem. Sci.* **12**, 301 (1987).
38. K. Taira and S. J. Benkovic, *J. Med. Chem.*, in press.
39. C. Singh and S. J. Benkovic, unpublished results.
40. P. J. Carter, G. Winter, A. J. Wilkinson, A. R. Fersht, *Cell* **38**, 835 (1984).
41. D. M. Lowe, G. Winter, A. R. Fersht, *Biochemistry* **26**, 6038 (1987).
42. A. R. Fersht, R. J. Leatherbarrow, T. N. C. Wells, *Trends Biochem. Sci.* **11**, 321 (1986).
43. D. A. Estell *et al.*, *Science* **233**, 659 (1986).
44. C. A. Fierke and W. P. Jencks, *J. Biol. Chem.* **261**, 7603 (1986).
45. A. J. Briggs *et al.*, *J. Am. Chem. Soc.* **106**, 6200 (1984).
46. H. B. Burgi and J. D. Dunitz, *Acc. Chem. Res.* **16**, 153 (1983).
47. Y. D. Wu and K. N. Houk, *J. Am. Chem. Soc.* **109**, 2226 (1987).
48. ———, personal communication.
49. K. Taira, C. A. Fierke, J.-T. Chen, K. A. Johnson, S. J. Benkovic, *Trends Biochem. Sci.* **12**, 275 (1987).
50. We thank J.-T. Chen, R. Mayer, K. Taira, K. Johnson, J. Andrews, C. Singh, K. Houk, and Y.-D. Wu for their help and involvement in this work. We also thank W. A. Goddard III for use of the computer graphics facility for graphical displays. This work was supported in part by NIH grant GM24129 and DOE-ECUT 49-242-E0403-0-3550. C.A.F. is a NIH postdoctoral fellow.

Manufacturing Innovation and American Industrial Competitiveness

STEPHEN S. COHEN AND JOHN ZYSMAN

An erosion of manufacturing capacities has contributed substantially to America's trade problems. The difficulty lies not in U.S. machines and technology, but in U.S. strategies for automation and the goals American firms seek to achieve through production innovation. Mass production and administrative hierarchies created the basis for American industrial preeminence in the years after World War II. There is substantial evidence that American firms have been unable to adopt or adapt to the production innovations emerging abroad. A sustained weakness in manufacturing capabilities could endanger the technology base of the country.

A GROWING DEBATE ON AMERICAN COMPETITIVENESS AND productivity has focused attention on manufacturing and manufacturing innovation (*1*). The scale and composition of the trade deficits of the past few years are the most prominent indicator that the competitive position of the American economy is weakening (*2*). The debate is about why the deficits have developed and what they mean. Our position is that much of the problem lies in an erosion of American manufacturing skills and capacities. If our position is correct, traditional economic remedies cannot in themselves reverse the decline in America's position in the international economy.

The huge trade deficits of the 1980s were driven by sharp increases in the value of the dollar that priced American goods out of world markets and made imports a bargain. The inflow of funds to finance the budget deficits pushed the exchange rate up. Consequently, some economists argue, the problem is fundamentally one of mistaken domestic macroeconomic policy. The process that created the trade deficits is reversible: reduce the budget deficit, thereby reducing demand for foreign borrowings to finance it, thereby reduce the trade deficit. To us this view is not so much wrong as it is limited and limiting.

Fifteen years ago this traditional remedy worked; devaluation rapidly reversed trade flows. This time, however, it has not, at least not as expected. Since 1985, the dollar has lost about half its value against the yen, but the trade deficit has stubbornly refused to follow suit. Only at the end of 1987 was a monthly decline first registered: the deficit fell to $13 billion, itself a record just a few months earlier. Certainly there is some price for the dollar at which imports would dry up and exports explode—if people had confidence that the exchange rate advantage would last. But balancing our external trade account is not the only objective. All nations, even the poorest, eventually do. The trick is to do it with high and rising incomes: that is the definition of national competitiveness (*3*). A permanently falling dollar translates into a continually impoverishing America. Clearly something new is affecting America's position in the international economy. What is it?

First, we have new competitors. The most important are Japan and Asia's newly industrializing countries. Japan's trade pattern is different from those of other advanced economies, for which intrasectoral trade has been the key to open trade. Japan uniquely has tended not to import in those sectors in which it is a major exporter (*3*, tables 8.1, 8.2, and 8.3). Second, the currencies of the Asian newly industrializing countries with whom we run major trade deficits have not risen against the dollar to the extent that the yen and European currencies have.

Most important, the United States once had dominant positions in product and production. We made products others could not make or could not begin to make competitively. Consequently, high wages and a high dollar did not displace us from markets. That situation has changed. In more technical terms, the price elasticities of American imports and exports have changed (*2*).

In the past 2 years the soaring yen has confronted Japan with a currency shock similar to the one we faced in 1981. A comparable percentage rise in the dollar flattened U.S. industrial investment and

The authors are professors at the University of California, Berkeley, CA 94720, where they are directors of the Berkeley Roundtable on the International Economy (BRIE).